Electronic Supplementary Material (ESI) for Journal of Materials Chemistry A.

In-situ hierarchical pore engineering in small pore zeolite via methanol-mediated NH_4F etching

Youdong Xing, Guangchao Li*, Zezhou Lin, Zhihang Xu, Haitao Huang, Ye Zhu, Shik Chi Edman Tsang, Molly Meng-Jung Li*

Youdong Xing, Guangchao Li, Zezhou Lin, Zhihang Xu, Haitao Huang, Ye Zhu, Molly Meng-Jung Li
Department of Applied Physics, The Hong Kong Polytechnic University, Hung Hom, Hong Kong (P. R. China)
E-mail: molly.li@polyu.edu.hk, guangchao.li@polyu.edu.hkmolly.li@polyu.edu.hk
Shik Chi Edman Tsang
Wolfson Catalysis Centre, Department of Chemistry, University of Oxford, Oxford OX1 3QR, U.K.

1. Experimental Sections and Characterizations

1.1 Samples preparation

A commercial SSZ-13 zeolite (from Shandong Dengzhuo Chemical Co., Ltd., Si/Al = 9.3) was used in this study. The etching process with the methanol-mediated NH_4F method was carried out as follows: typically, 1g of the zeolite was dispersed in a concentration range (3.5 wt%, 1.7 wt%, and 0.5 wt%) of NH_4F (Aladdin, 98.0 wt%) methanol (Sigma-Aldrich, ≥99.9%) solution at room temperature for 1 hour under mechanical stirring for homogeneous mix in a 20 ml Teflon reactor. Subsequently, the reactor was transferred into an oil bath at 50°C to etch the zeolite under mechanical stirring for 12 h. Then the resulting samples were named MF-3.5, MF-1.7, and MF-0.5, respectively. The solid products were thoroughly washed with distilled water several times and dried at 80°C overnight.

To preserve the etched species for characterization, the samples by methanol evaporation were obtained as follows: typically, 1g of the zeolite was dispersed in a concentration range (3.5 wt%, 1.7 wt%, and 0.5 wt%) of NH_4F methanol solution at room temperature for 1 hour under mechanical stirring in a 20 ml Teflon reactor. Subsequently, the reactor was transferred into an oil bath at 50°C to etch the zeolite when evaporating the methanol under mechanical stirring. The resulting dried samples were labelled as MF-3.5E, MF-1.7E, and MF-0.5E, respectively.

Synthesis of the counterpart with a conventional NH_4F aqueous solution under equivalent conditions with MF-3.5 except for aqueous solution. The obtained sample is denoted as WF-3.5.

1.2 Characterizations

The microstructure and morphology of the pristine SSZ-13 and synthesized samples were measured by Field Emission Scanning Electron Microscope (FESEM, Tescan MAIA3), and the chemical composition was analyzed with SEM (TESCAN VEGA3) in combination with an X-ray spectrometer EDX detector.

Transmission electron microscopy (TEM) and energy-disperse X-ray (EDX) mapping were carried out on a JEOL JEM-2100F at 200 kV, using the holey carbon-coated copper grid.

The crystallinity and phase purity of the samples were determined by powder X-ray diffraction (PXRD) on a Rigaku SmartLab 9 kW diffractometer using Cu Kα radiation (λ = 1.5418 Å) in the 2θ range 5-60º with scanning steps of 0.08º s^{-1}. The crystallinity was estimated by comparing the total area of the reflection peaks in the 2θ range of 9.6–21° to that of the pristine SSZ-13 assuming 100% crystallinity.[1]

X-ray photoelectron spectroscopy (XPS) measurements were conducted using a Thermo Fisher Esca Lab. The spectra were calibrated by observing the adventitious C 1s peak at around 284.8 eV for all the tested samples.

The wettability of the SSZ-13 zeolite surface for water and methanol was measured using a contact angle goniometer (LAUDA Scientific GmbH, LSA-100).

Argon (87K) and nitrogen (77K) adsorption/desorption measurements were carried out on a Micromeritics ASAP 2460 and Micromeritics 2020 analyzer, respectively, after the samples were degassed at 300°C for 12 hours. The specific surface area and pore volumes were determined by Brunauer-Emmett-Teller and t-plot methods, respectively. The mesopore size distribution was obtained from the adsorption branch of the isotherm based on the Barrett-Joyner-Halenda (BJH) method.

All NMR experiments were performed on a Jeol ECZ500R spectrometer equipped with a 3.2-, 8-mm MAS probe or 5mm liquid-state probe, with resonance frequencies of 495.13, 465.89, 129.02, and 98.37 MHz for ^{1}H, ^{19}F, ^{27}Al, and ^{29}Si nuclei, respectively. The deconvoluted spectra were performed with the DMFIT software.

^{1}H Magic Angle Spinning (MAS) SSNMR spectra were acquired on a 3.2 mm probe with a spinning rate of 10 kHz, a pulse width of 2.43 μs (ca. π/2 pulse), a recycle delay of 5 s, and 32 scans. 2D ^{1}H-^{1}H double quantum-single quantum (DQ-SQ) MAS SSNMR experiment with the POST-C7 pulse sequence to excite and reconvert DQ coherences. The increment interval in the indirect dimension (t1) was set to 20 μs, and 128 t1 increments and 64 scan accumulations for each t1 increment was used. The dehydrated samples were performed at a pressure below 10^{-3} Pa under 723 K for 12 h before the measurements. The chemical shifts of ^{1}H were referenced to solid adamantane at 1.7 ppm.

^{19}F MAS SSNMR spectra were recorded with a spinning rate of 18 kHz on the 3.2 mm probe head. The Hahn echo sequence was employed to remove a broad probe signal. The delay between the π/2 and π pulses was synchronized with the spinning frequency ($V_r = 1/\tau = 18$ kHz) and was chosen as 55.56 μs. For such a low value, the Hahn echo experiments can give the relative proportions of the different species. The spectra were accumulated for 64 scans with a recycle delay of 5 s. Chemical shifts were referenced to CF_3COOH as an external standard at -76.55 ppm. ^{19}F liquid-state NMR spectrum was recorded with a 5 mm liquid-state probe. The chemical shifts of ^{19}F were referenced to $C_6H_5CF_3$ (trifluoro-toluene) at -63.72 ppm.

The single-pulse ^{27}Al MAS SSNMR spectra were collected at a spinning rate of 12 kHz with a recycle delay of 0.5 s and 1024 scans. A small flip angle (π/12) associated with a short pulse duration (0.16 μs) was used to ensure the homogeneous excitation of the whole signals for the acquisition of a quantitative NMR spectrum. In the 2D ^{27}Al multiple-quantum (MQ) MAS z-filtering SSNMR experiments, the optimized pulse widths were p1 = 5.0μs, p2 = 1.4μs, and p3 = 6μs. The spectra were collected with 128 t1 increments and 256 scan accumulations for each t1 increment. The SSNMR parameters determined from the ^{27}Al MQ MAS SSNMR spectra were used to simulate the ^{27}Al MAS SSNMR spectra for quantitative analysis on the different Al sites. The $^{1}H \rightarrow ^{27}Al$ cross-polarization magic angle spinning ($^{27}Al(^{1}H)$ CP MAS SSNMR) and $^{1}H \rightarrow ^{27}Al$ heteronuclear correlation SSNMR spectra (2D $^{27}Al(^{1}H)$ HETCOR SSNMR) were performed at a spinning speed of 12 kHz with short contact times of 0.05 ms and 0.5 ms, respectively, a recycle delay of 1 s. ^{1}H TPPM decoupling was employed during the ^{27}Al signal acquisition (pulse length 2.43 μs, rf field ca. 103 kHz). $^{27}Al(^{19}F)$ CP MAS and $^{27}Al(^{19}F)$ HETCOR SSNMR spectra were obtained with a contact time of 0.05 ms with a recycle delay of 1 s. The chemical shifts of ^{27}Al were referenced to a 1.0 M aqueous $Al(NO_3)_3$ at 0 ppm.

The single-pulse ^{29}Si MAS NMR spectra were acquired at a spinning rate of 4 kHz on an 8 mm probe head by a single π/2 pulse with 7.61 μs width and a recycle delay of 60 s and 24 scans. $^{29}Si(^{1}H)$ CP MAS and $^{29}Si(^{1}H)$ HETCOR SSNMR spectra were performed with an RF field of 23 and 18 kHz for ^{29}Si and ^{1}H, respectively, with a contact time of 4 and 0.4 ms. A total of 40 t1 slices with 256 scans were recorded for the 2D experiment. ^{1}H TPPM decoupling was applied during the ^{29}Si signal acquisition (pulse length 8.67 μs, rf field ca. 33 kHz). ^{29}Si chemical shifts were referenced to kaolinite.

2. Supplementary Figures and Tables

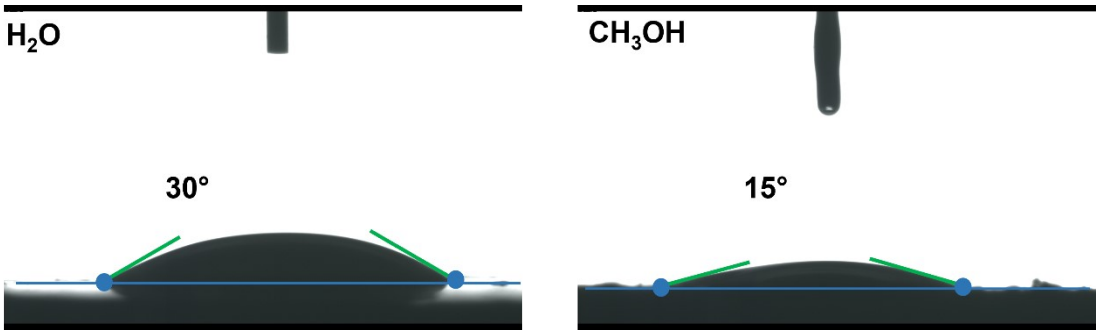

Figure S1. Contact angles of H_2O and CH_3OH with SSZ-13 zeolite. The lower contact angle of CH_3OH compared to water indicates that methanol possesses higher surface wettability than water.

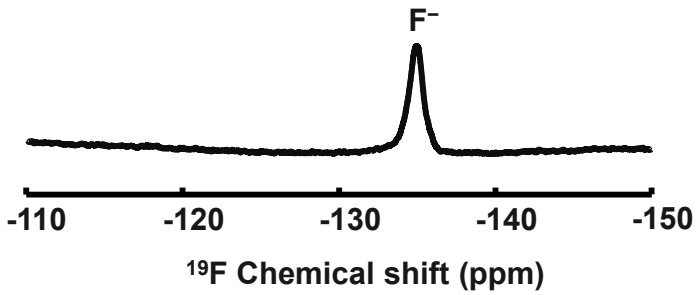

Figure S2. ^{19}F liquid NMR spectrum of 3.5 wt% NH_4F in ethanol, reveals a single peak of solvated F^-, suggesting ethanol can dissolve NH_4F and potentially offer similar functionality for the inactive transportation of NH_4F into the zeolite channel and in-situ hydrolysis activation.

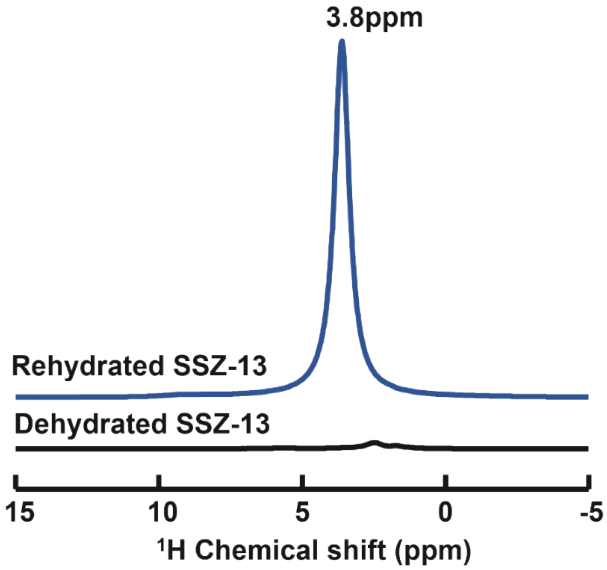

Figure S3. ^{1}H MAS SSNMR spectra of the dehydrated SSZ-13 at 450°C for 12 hours and the rehydrated SSZ-13 were obtained by exposing the dehydrated SSZ-13 in the SSNMR rotor to the atmosphere for three days. These experiments were conducted to verify the existence of H_2O in the SSZ-13 zeolite. A significant peak at 3.8 ppm after rehydration can be observed, indicating that the zeolite can accommodate a considerable amount of H_2O molecules.

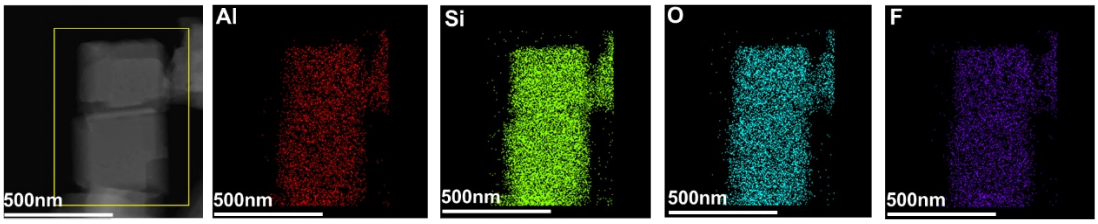

Figure S4. TEM image and EDX elemental mapping (Al, Si, O and F) in the selected zeolite matrix (seen in the yellow box of TEM image) for the SSZ-13 treated by 3.5 wt% NH_4F methanol solution under room temperature for 10min. The results show that F element is uniformly distributed throughout the crystal, suggesting the penetration of the NH_4F into the zeolite pores after NH_4F-methanol treatment.[2]

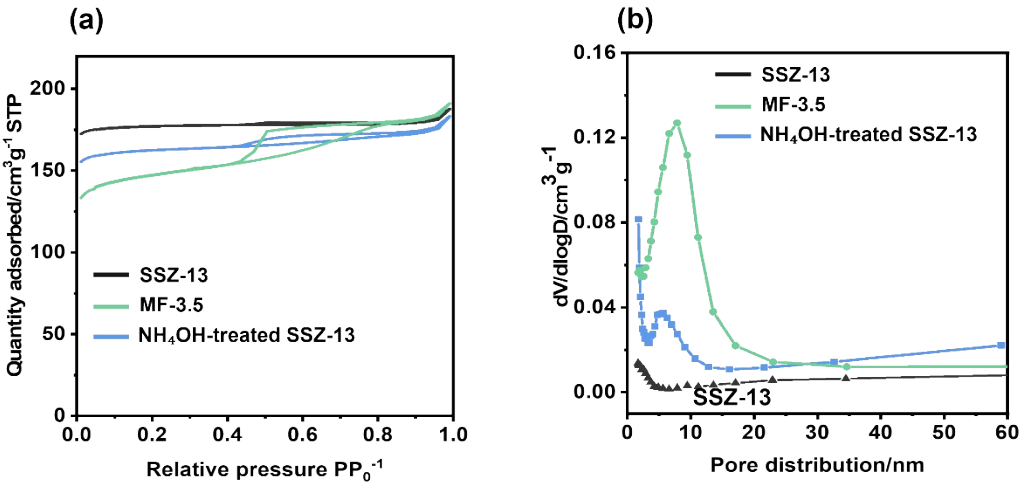

Figure S5. (a) N_2 adsorption/desorption isotherms of the SSZ-13, MF-3.5, and NH_4OH-treated SSZ-13. (b) The corresponding mesopore size distribution is derived from the adsorption branch of the isotherms based on the BJH model.

Table S1. Textural data was obtained from the N_2 isotherms of the pristine SSZ-13, MF-3.5 and NH_4OH-treated SSZ-13.

Sample	[a] S_{BET} ($m^2 g^{-1}$)	[b] S_{meso} ($m^2 g^{-1}$)	[c] V_{mic} ($cm^3 g^{-1}$)	[d] V_{meso} ($cm^3 g^{-1}$)
SSZ-13	530	17	0.27	0.02
MF-3.5	454	85	0.19	0.11
NH_4OH treated SSZ-13	491	32	0.28	0.04

[a] Total surface area. [b] Mesopore surface area, t-plot. [c] Micropore volume, t-plot. [d] Mesopore volume, (V_{total}-V_{mic}).

The pH of the 3.5 wt% NH_4F methanol solution indicates weak alkalinity (pH 9.1-9.3). Hence, the potential alkaline etching ability of NH^{4+} upon dissociation from NH_4F to form a weak base should be considered, as it may contribute to the etching process. To investigate the role of solution alkalinity in mesopore formation, we treated SSZ-13 zeolite in an ammonia solution with the same molar concentration and etching conditions (50°C for 12 hours) as sample MF-3.5. The resulting SSZ-13 in the ammonia solution exhibited stronger alkalinity (pH = 11.7). However, the NH_4OH-treated SSZ-13 only displayed a small hysteresis loop in the N_2 adsorption/desorption isotherm (**Figure S5a**), indicating minimal mesopore formation (0.04 $cm^3 g^{-1}$, **Table S1**) and a weak peak in the pore size distribution (**Figure S5b**). In contrast, sample MF-3.5 obtained from NH_4F-methanol treatment exhibited a substantial amount of mesopores (0.11 $cm^3 g^{-1}$, **Table S1**). Therefore, we conclude that the etching process and mesopore formation are primarily attributed to the effects of NH_4F rather than alkaline etching.

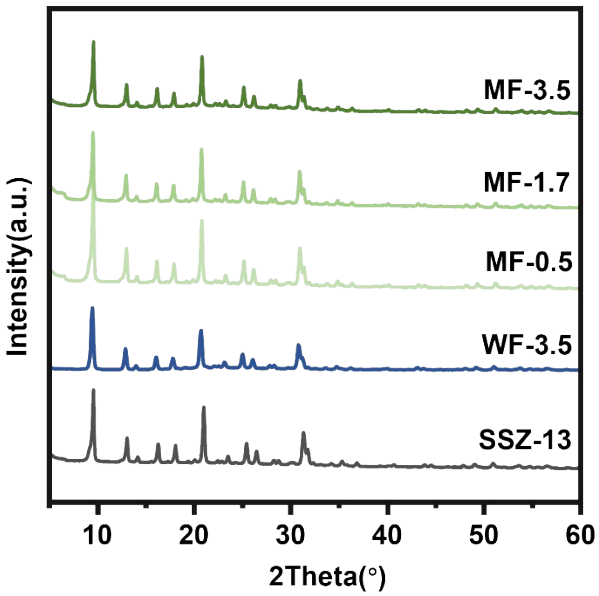

Figure S6. XRD patterns of the SSZ-13 and NH_4F-treated samples reveal that all prepared samples exhibit a high degree of crystallinity with the typical CHA topology and no amorphous crystal formation.

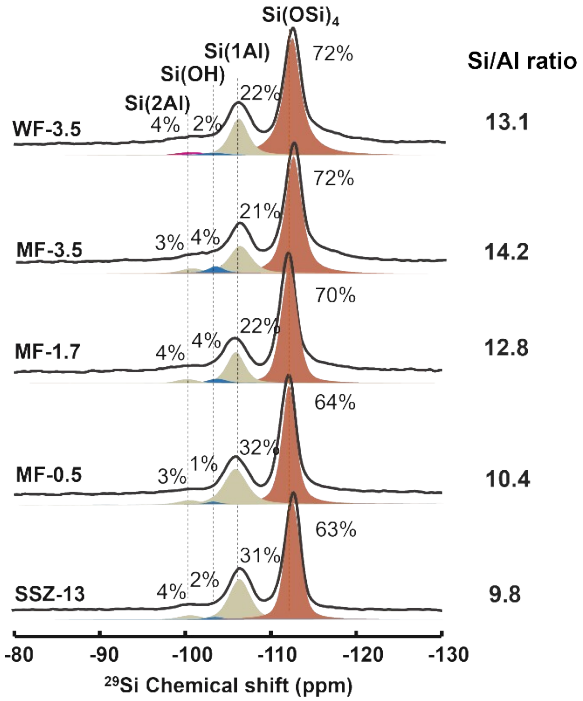

Figure S7. ^{29}Si MAS SSNMR spectra with decomposed peaks of specific Si and corresponding contents in the pristine and MF-0.5~3.5 samples. Si/Al ratio is determined with the equation: $\sum_{n=0}^{4} I_{Si(OAl)_n} / 0.25 \sum_{n=0}^{4} nSI_{Si(OAl)_n}$.

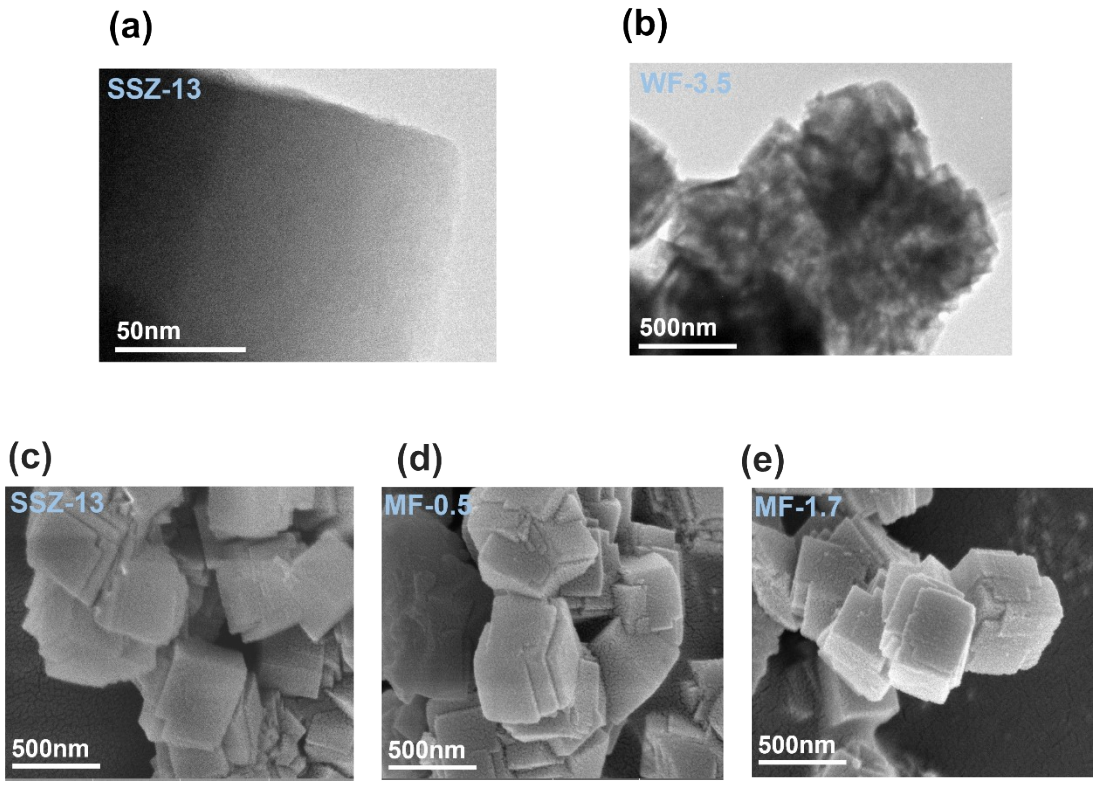

Figure S8. TEM images of (a) SSZ-13 and (b) WF-3.5. SEM images of (c) SSZ-13, (d) MF-0.5 and (e) MF-1.7 samples.

The SSZ-13 crystal exhibits no visible cracks or defects and displays sharp edges, indicating a high degree of structural order (**Figure S8a**). In contrast, the sample of WF-3.5, obtained from the conventional NH_4F-water etching method, displays large mesopores or macropores within severely damaged SSZ-13 crystals, making it difficult to distinguish the crystal edges (**Figure S8b**). SEM images of samples MF-0.5 and MF-1.7 (**Figure S8d-e**), obtained via the methanol-mediated NH_4F etching method, exhibit smooth crystal surfaces, similar to that of the pristine SSZ-13 (**Figure S8c**), indicating the crystal surfaces are not preferentially etched.

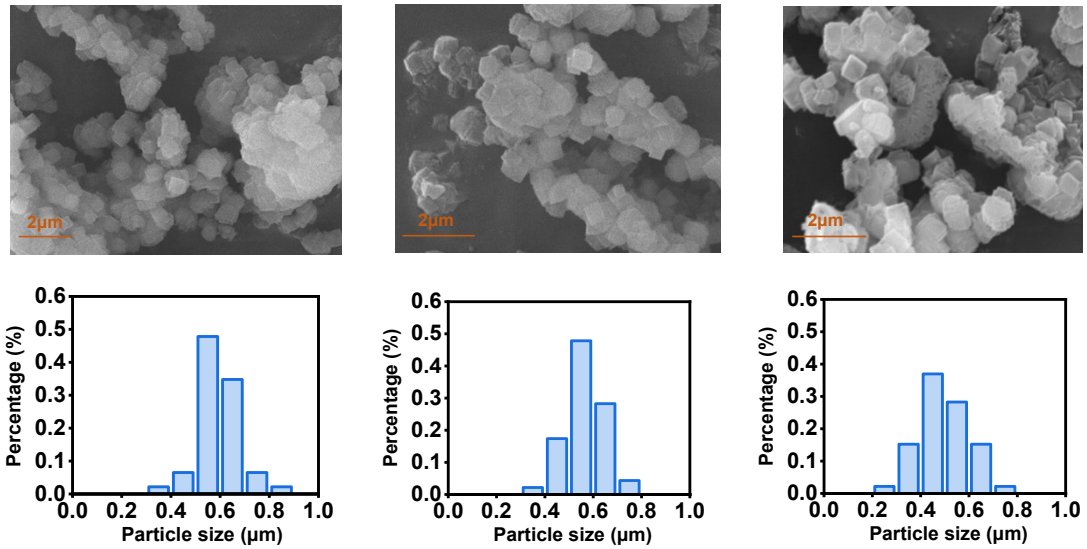

Figure S9. SEM images of the SSZ-13, MF-3.5 and WF-3.5 samples and the corresponding crystallite particle size distribution, which reveals that the MF and WF sample has a similar particle size distribution to that of the SSZ-13 zeolite.

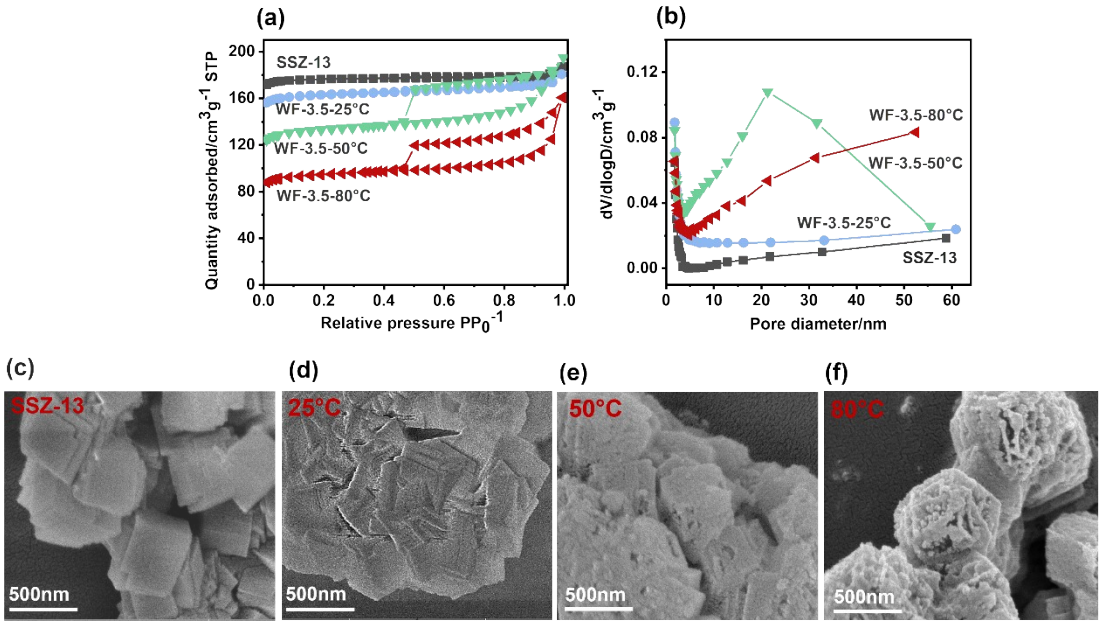

Figure S10. (a) N_2 adsorption/desorption isotherms and (b) mesopore size distribution (based on the BJH model) of SSZ-13 and NH_4F-water treated samples at 25°C, 50°C and 80°C. Corresponding SEM images are shown in (c-f).

Table S2. Textural data was obtained from the N_2 isotherms of the pristine SSZ-13 and WF-3.5-25°C~80°C.

Sample	*[a] S_{BET} ($m^2 g^{-1}$)*	*[b] S_{meso} ($m^2 g^{-1}$)*	*[c] V_{mic} ($cm^3 g^{-1}$)*	*[d] V_{meso} ($cm^3 g^{-1}$)*
SSZ-13	530	17	0.27	0.02
WF-3.5-25°C	492	33	0.24	0.04
WF-3.5-50°C	407	50	0.18	0.12
WF-3.5-80°C	290	38	0.13	0.12

[a] Total surface area. [b] Mesopore surface area, t-plot. [c] Micropore volume, t-plot. [d] Mesopore volume, (V_{total}-V_{mic}).

To investigate the possibility of obtaining a uniformly distributed mesoporous structure by varying the temperature in the NH_4F-water etching system, a series of experiments were conducted at different temperatures (25°C, 50°C, and 80°C)

The undetectable hysteresis loops from the N_2 adsorption/desorption isotherm (**Figure S10a)** and the negligible mesopores volume (0.04 cm^3/g, **Table S2**) for SSZ-13 before and after being treated with NH_4F-water solution at 25°C suggest that formation of detectable mesopore hardly occurs under the low-temperature condition. However, we have observed that even at lower temperatures of 25°C, the surface of the SSZ-13 zeolite was etched, resulting in unclear particle edges (**Figures S10c-d**), although no obvious mesopore structure was observed from N_2 adsorption/desorption isotherms. As the temperature increased from 25°C to 80°C, the presence of mesopores (hysteresis loops) became clearer, and the surface became rough with the formation of larger pores and holes (**Figures S10 and Table S2**). As demonstrated by the N_2 adsorption/desorption isotherms of WF-3.5-50°C (**Figure S10a),** an obvious hysteresis loop is observed and mesopore volume is estimated to be 0.12 cm^3/g (**Table S2**). Additionally, the broad pore size distribution ranging from 2 nm to 60 nm (**Figure S10b)** indicates that the etching process is non-uniform. As the etching temperature increases, a more severe etching and pore formation is observed in the sample treated at 80°C (Figures S10a, b and f).

This suggests that the diffusion of the etching species in the NH4F-water treatment is difficult, leading to etching initiation at the outer surface of the zeolite particles. Therefore, adjusting the etching temperature from 25°C to 80°C for the NH_4F-water etched SSZ-13 did not result in well-distributed mesopores, and the zeolite outer surfaces are etched in all the obtained WF samples regardless of the temperature.

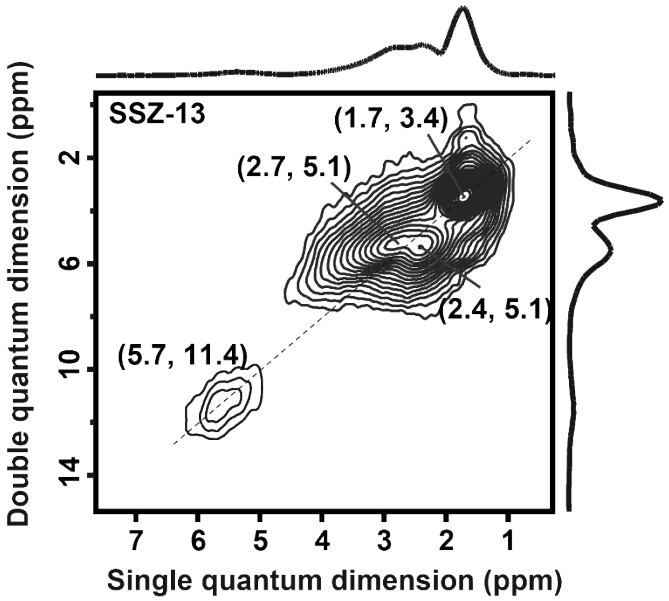

Figure S11. ^{1}H DQ MAS SSNMR spectrum of the dehydrated SSZ-13 zeolite.

^{1}H DQ MAS SSNMR spectrum is used to confirm the specific structure of Al(IV)-2 species, which is related to the number of OH groups present in Al(IV)-2. The absence of an autocorrelation peak at (2.7, 5.4) ppm suggests that the 2.7 ppm signal of Al(IV)-2 can be attributed to framework-associated Al with only a single OH group, specifically, $(SiO)_3Al(OH)$ species.[5] Additionally, the autocorrelation peak at (1.7, 3.4) ppm suggests spatial proximity between the protons of silanol groups. Another autocorrelation peak at (5.7, 11.4) ppm is assigned to trace strong adsorption water molecules. The paired signal at (2.7, 5.1) ppm and (2.4, 5.1) ppm indicates the correlations between two protons of Al(IV)-2 and extra-framework Al hydroxyl, respectively.[5]

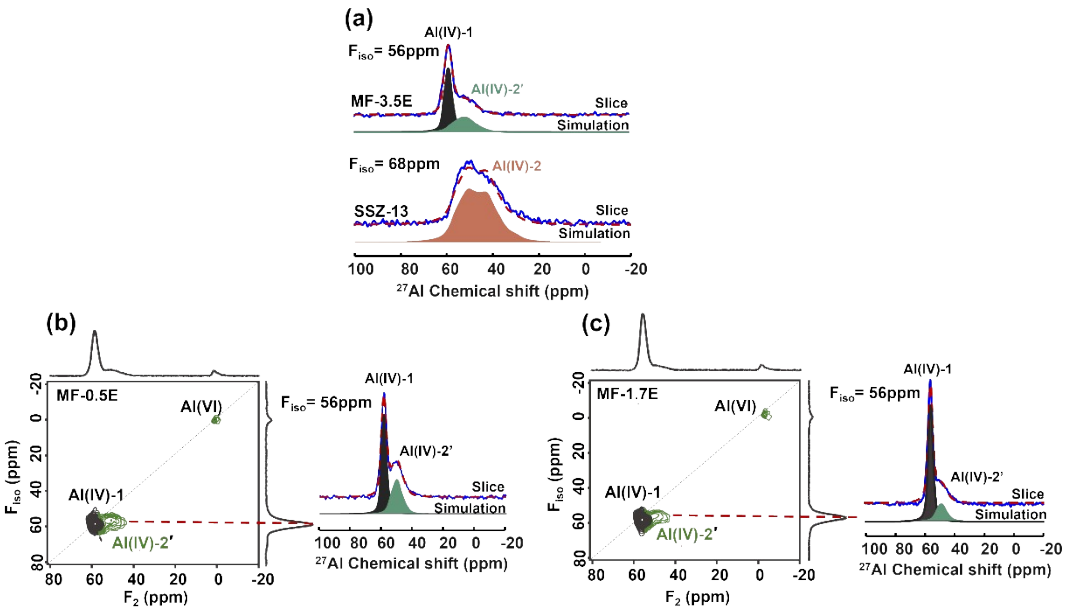

Figure S12. (a) Selected slices with simulations extracted from the ^{27}Al MQ MAS SSNMR spectra of SSZ-13 and MF-3.5E samples in **Figures 3b-c**. ^{27}Al MQ MAS SSNMR spectra of (b) the MF-0.5E and (c) MF-3.5E and corresponding slices with simulations at selected sites.

Table S3. Isotropic chemical shifts (δ_{iso}), the quadrupolar coupling constant (C_q), and concentration of the Al sites in the SSZ-13 zeolite and MF-0.5E~3.5E samples.

		Al(IV)-1	Al(IV)-2	Al(VI)
SSZ-13				
	δ_{iso}(ppm)[a]	58.6	60.2	\
	C_q (MHz)[b]	2.5	5.9	
	Al Conc.(%)	36	64	
F-0.5E			**Al(IV)-2′**	
	δ_{iso}(ppm)	58.7	54.4	3.2
	C_q (MHz)	2.6	4.5	2.2
	Al Conc.(%)	36	51	13
F-1.7E				
	δ_{iso}(ppm)	58.3	54.4	3.5
	C_q (MHz)	2.6	4.4	2.4
	Al Conc.(%)	36	39	25
F-3.5E				
	δ_{iso}(ppm)	58.6	54.7	3.0
	C_q (MHz)	2.6	4.4	2.7
	Al Conc.(%)	36	30	34

[a] Isotropic chemical shift is calculated from the equation $\delta_{iso} = (17\delta_{F1} + 10\delta_{F2})/27$, δ_{F1} and δ_{F2} are the center of gravity of each species measured along the direct dimension F2 and isotropic dimension F1 on MQ spectra (**Figures 3b-c and Figure S12**), respectively. [b] The quadrupolar coupling constant (C_q) is extracted from the slice of the MQ spectra by simulating with the DMFIT program on the corresponding second-order quadrupolar line shape (Ƞ= 0.6).[6]

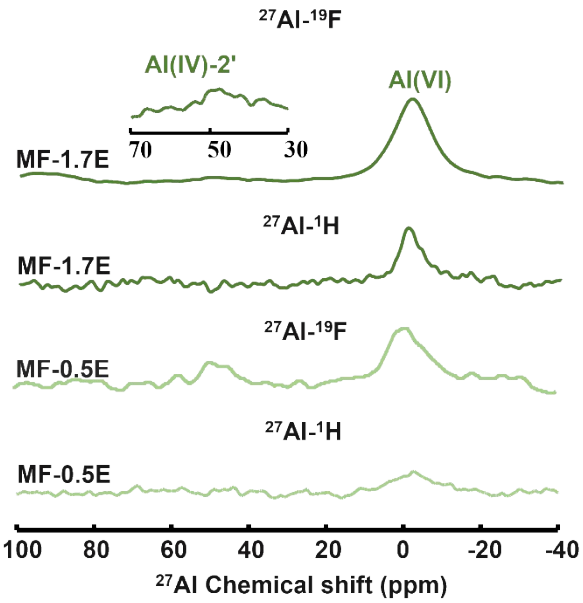

Figure S13. $^{27}Al(^{1}H)$ and $^{27}Al(^{19}F)$ CP MAS SSNMR spectra of the MF-0.5E and MF-1.7E samples.

The $^{27}Al(^{19}F)$ CP MAS SSNMR spectra of the MF-0.5E and MF-1.7E samples reveal the appearance of a signal at 40-60 ppm, which indicates a short distance between Al and F atoms in Al(IV)-2' sites. Furthermore, the Al(IV)-2 signal (20-60 ppm) in $^{27}Al(^{1}H)$ CP MAS SSNMR spectra of both samples disappears compared to the pristine SSZ-13 (as shown in **Figure 3d**). This finding suggests that the OH group of $(SiO)_3Al(OH)$ (i.e., Al(IV)-2) in SSZ-13 is consumed, resulting in the conversion towards $(SiO)_3Al$-F (i.e., Al(IV)-2') after NH_4F-methanol treatment.

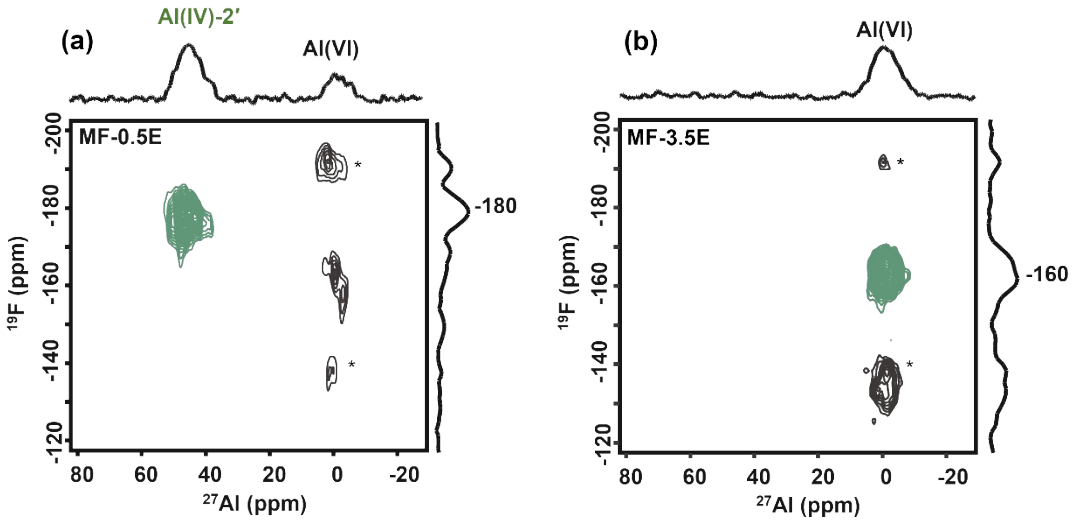

Figure S14. ^{27}Al(^{19}F) HETCOR MAS SSNMR spectra of (a) MF-0.5E and (b) MF-3.5E with a contact time of 50us. The spinning sidebands are labelled *.

^{27}Al(^{19}F) HETCOR MAS NMR spectra, which can provide valuable information on the spatial proximity and connectivity of the specific ^{19}F and ^{27}Al nuclei in the zeolite, were used to assist the assignment of signals that appeared in 1D ^{19}F MAS NMR spectra (**Figure 4b**). For the MF-0.5E sample with the most Al(IV)-2' sites ($(SiO)_3$Al-F) among the MF samples, the cross-peak (marked by green) between ^{19}F resonance at -180 ppm and ^{27}Al resonance of Al(IV)-2' sites (at about 40~60 ppm) in **Figure S14a** indicates the F atom in proximity to the Al atom of Al(IV)-2' sites. Thus the peak at -180 ppm can be attributed to Al(IV)-2' species. This similar assignment was also reported in Y zeolite possessing F-bearing tetrahedral Al, $(SiO)_3$Al-F.[7]

For the MF-3.5E sample, a strong cross-peak between the ^{19}F resonance at -160 ppm and the ^{27}Al resonance of Al(VI) sites at 0 ppm is observed (**Figure S14b)**, indicating that the ^{19}F signal at -160 ppm is attributed to Al(VI) sites. The absence of the correlation peak between ^{19}F resonance at -180 ppm and ^{27}Al resonance of Al(IV)-2' sites can be explained by the lower concentration of Al(IV)-2' species in the sample.

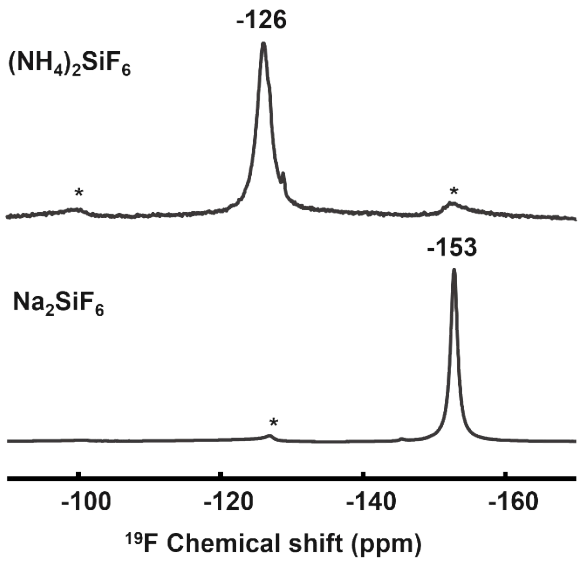

Figure S15. ^{19}F MAS SSNMR spectra of standards, Na_2SiF_6 and $(NH_4)_2SiF_6$. The spinning sidebands are labelled *.

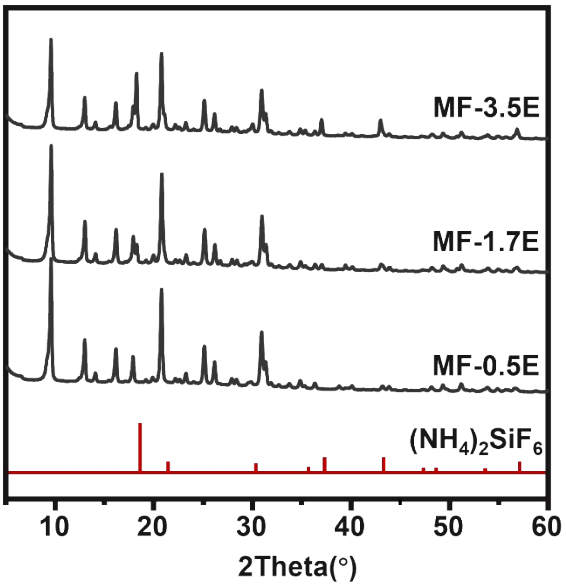

Figure S16. XRD patterns of MF-0.5E, -1.7E and -3.5E samples.

From the XRD patterns, the MF-0.5E sample displays solely the characteristic peak of the CHA structure, while with increasing NH_4F concentration, the characteristic peak of $(NH_4)_2SiF_6$ emerges (in MF-1.7E) and increases in intensity. These observations indicate that the framework Si atoms are gradually extracted into non-framework species during the NH_4F treatment process.

a)

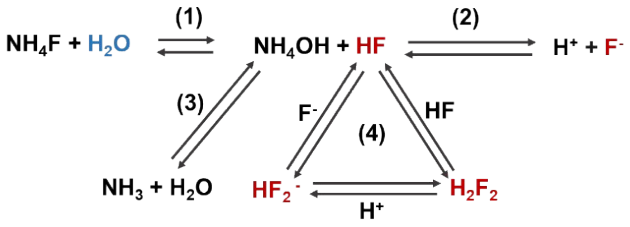

b)

Scheme S1. Equilibrium of NH_4F in (a) water[8] and (b) methanol solution.

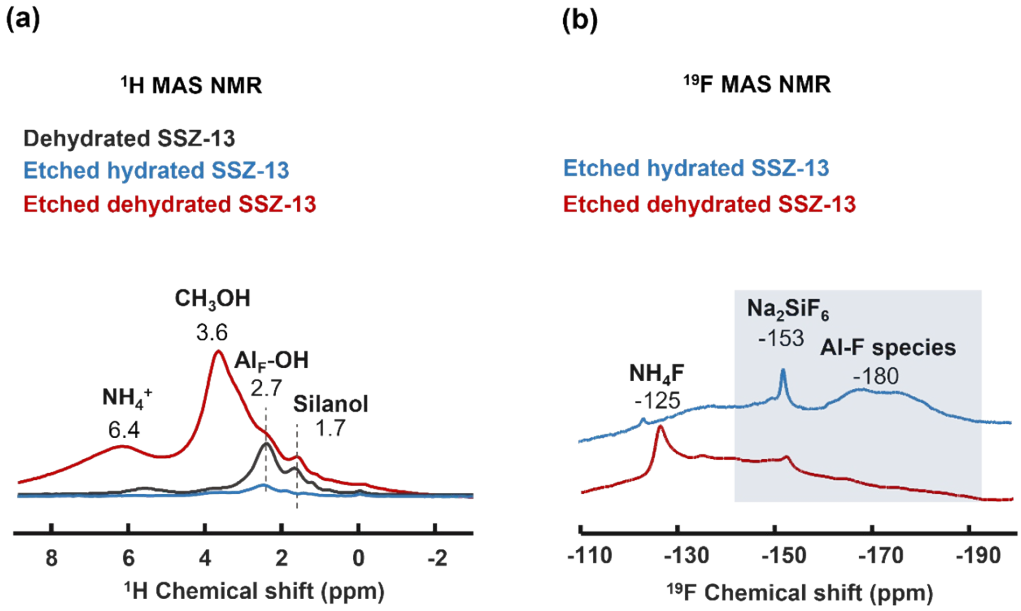

Figure S17. ^{1}H and ^{19}F MAS SSNMR spectra of the dehydrated SSZ-13(black line), etched hydrated SSZ-13 (blue line) and etched dehydrated SSZ-13 (red line) with 0.5 wt% NH_4F methanol solution.

In our methodology, the existence of water in zeolite plays a crucial role in controlling the release of active etching species, as these species are generated only through the hydrolysis of F^- (**Scheme S1**). To support this conclusion, ^{1}H and ^{19}F SSNMR experiments were conducted for both hydrated and dehydrated SSZ-13 samples treated with 0.5wt% NH_4F in methanol (**Figure S17**). Compared to the pristine SSZ-13, the ^{1}H peaks for Si-OH and Al-OH exhibit a significant decrease in the etched hydrated SSZ-13 but remain unchanged in the etched dehydrated SSZ-13 (**Figure S17a**), indicating that solvated F^- species in the dehydrated SSZ-13 are unable to react with Si-OH and Al-OH. This finding can be further supported by the corresponding ^{19}F SSNMR results, which show no obvious ^{19}F peaks for Si-F (Na_2SiF_6) and Al-F species (Al(IV)-2' sites) in the etched dehydrated SSZ-13 (**Figure S17b**). Therefore, from the above results, we can conclude that water is essential to initiate the hydrolysis reaction, generating highly reactive etching species that are responsible for modifying the porosity of zeolites.

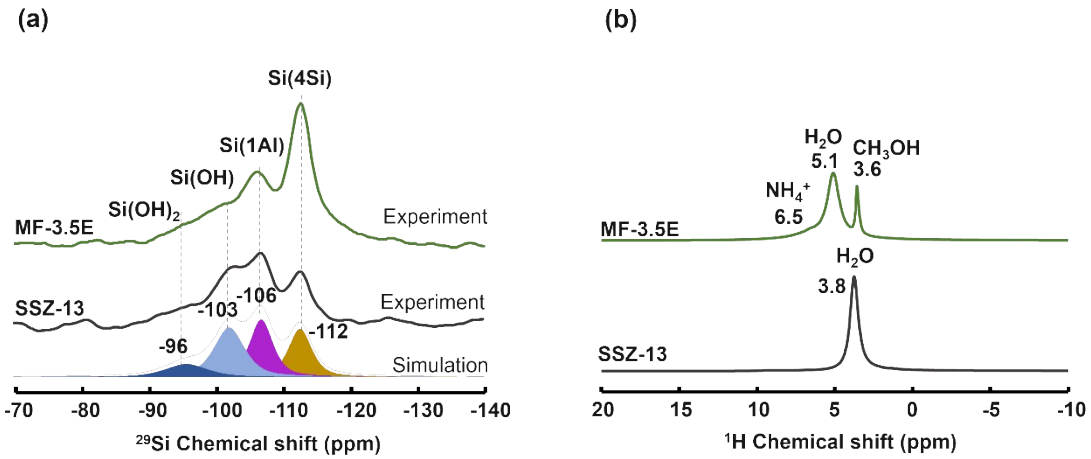

Figure S18. (a) $^{29}Si(^{1}H)$ CP MAS SSNMR spectra (a contact time of 4 ms) and (b) ^{1}H MAS NMR of the SSZ-13 and the MF-3.5E sample.

$^{29}Si(^{1}H)$ CP MAS SSNMR spectra of the SSZ-13 and the MF-3.5E sample exhibit four distinct peaks at -96, -103, -106, and -112 ppm, which are attributed to $Si(OH)_2$, Si(OH), Si(1Al), and Si(4Si), respectively, according to the literature[9].

^{1}H MAS SSNMR spectrum of the hydrated SSZ-13 reveals a prominent H_2O signal at 3.8 ppm, which has been confirmed in the dehydration/rehydration experiments (**Figure S3)**. After NH_4F treatment, the water peak shifts to 5.1 ppm, which may result from the bound water with extra-framework species. Additionally, the peaks at 3.6 ppm and 6.5 ppm are attributed to residual CH_3OH during evaporation treatment and NH_4^+, respectively.[10-11]

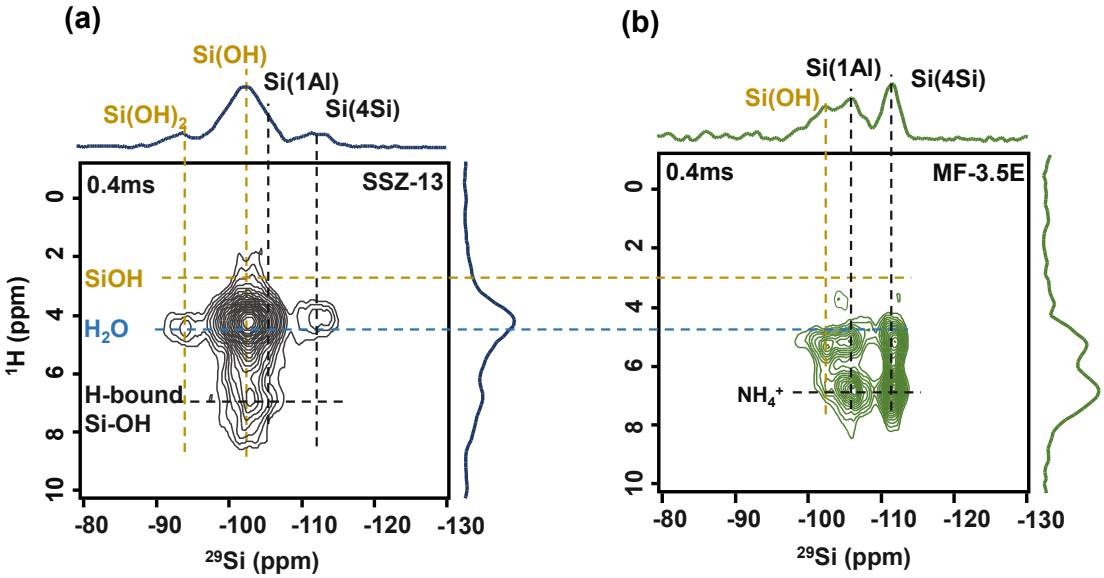

Figure S19. $^{29}Si(^{1}H)$ HETCOR MAS SSNMR spectra of (a) SSZ-13 and (b) MF-3.5E with a contact time of 0.4 ms.

$^{29}Si(^{1}H)$ HETCOR MAS SSNMR spectrum of the SSZ-13 zeolite (**Figure S19a**) with a contact time of 0.4 ms shows that the intensity of two correlation peaks between H_2O and silanol species (Si-$(OH)_2$ and Si-OH) remains virtually unchanged, compared to the case of the 4 ms contact time (**Figure 4c**). This indicates close spatial proximity between H_2O molecules and the silanols. On the other hand, there is a notable decrease in the intensity of the correlation peak between H_2O molecules and Si(4Si) units as the contact time is shortened, suggesting a long distance between them.

For the MF-3.5E sample, despite the reduction in contact time, the intensity of the correlation between NH_4^+ (H_2O) and Si(1Al)/Si(4Si) species remains relatively unchanged (**Figure 4c and Figure S19b**). This suggests a high degree of proximity between these entities.

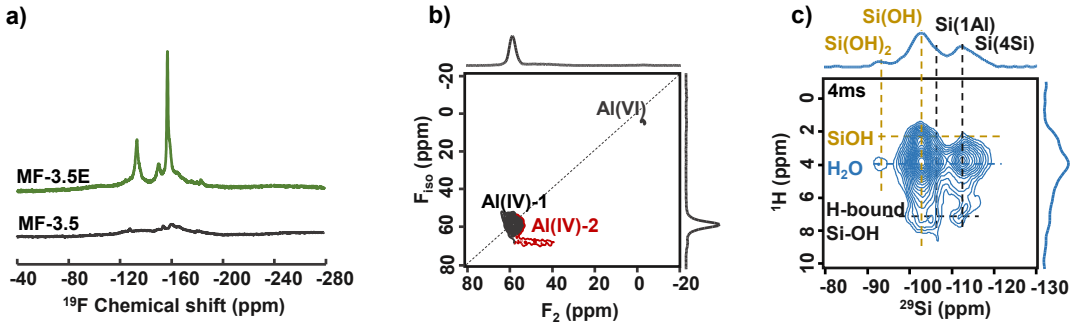

Figure S20. (a) ^{19}F MAS SSNMR (spinning frequency= 12 kHz), (b) ^{27}Al MQ MAS SSNMR, and (c) ^{29}Si(^{1}H) HETCOR MAS SSNMR (with a contact time of 4 ms) spectra of the MF-3.5 sample.

To verify that the F species, including $(NH_4)_2SiF_6$, $(NH_4)_2SiF_6$, extra-framework Al-F and framework Si-F and Al-F species, formed in the MF-3.5E sample are removed after water washing, we characterize its corresponding MF-3.5 sample by SSNMR spectroscopy. The ^{19}F MAS SSNMR spectrum of MF-3.5 shows a very low signal compared to MF-3.5E without washing (shown in **Figure S20a**), indicating the effective removal of F species.

2D ^{27}Al MQ MAS SSNMR spectrum of the MF-3.5 sample (**Figure S20b)** shows the reappearance of the Al(IV)-2 peak and the absence of Al(IV)-2' signal, in comparison to that of the MF-3.5E sample (**Figure 3c**). This suggests that the Al-F species in the MF-3.5E sample are converted back to Al-OH upon washing.

^{29}Si(^{1}H) HETCOR MAS SSNMR spectrum of the MF-3.5 sample (**Figure S20c)** displays that the reappearance of the correlation peak between H_2O and silanols (Si-$(OH)_2$ and Si-OH), compared to that of the MF-3.5E sample (**Figure 3c**), indicates the hydrolysis of the tetrahedral framework Si-F towards Si-OH species.

Based on the above results, we can confirm that the F species formed in the etching process can be removed after water washing.

3. References

1. Wardani, M. K.; Kadja, G. T.; Fajar, A. T.; Makertihartha, I.; Gunawan, M. L.; Suendo, V.; Mukti, R. R., Highly Crystalline Mesoporous SSZ-13 Zeolite Obtained Via Controlled Post-Synthetic Treatment. *RSC advances* **2019**, *9*, 77-86.
2. Qin, Z.; Cychosz, K. A.; Melinte, G.; El Siblani, H.; Gilson, J. P.; Thommes, M.; Fernandez, C.; Mintova, S.; Ersen, O.; Valtchev, V., Opening the Cages of Faujasite-Type Zeolite. *Journal of the American Chemical Society* **2017**, *139*, 17273-17276.
3. Babić, V.; Koneti, S.; Moldovan, S.; Nesterenko, N.; Gilson, J.-P.; Valtchev, V., Preparation of Hierarchical SSZ-13 by NH_4F Etching. *Microporous and Mesoporous Materials* **2021**, *314*, 110863.
4. Qin, Z.; You, Z.; Bozhilov, K. N.; Kolev, S. K.; Yang, W.; Shen, Y.; Jin, X.; Gilson, J. P.; Mintova, S.; Vayssilov, G. N., Dissolution Behavior and Varied Mesoporosity of Zeolites by NH_4F Etching. *Chemistry–A European Journal* **2022**, *28*, e202104339.
5. Fan, B.; Zhu, D.; Wang, L.; Xu, S.; Wei, Y.; Liu, Z., Dynamic Evolution of Al Species in the Hydrothermal Dealumination Process of Cha Zeolites. *Inorganic Chemistry Frontiers* **2022**, *9*, 3609-3618.
6. Xin, S.; Wang, Q.; Xu, J.; Chu, Y.; Wang, P.; Feng, N.; Qi, G.; Trébosc, J.; Lafon, O.; Fan, W., The Acidic Nature of "NMR-Invisible" Tri-Coordinated Framework Aluminum Species in Zeolites. *Chemical Science* **2019**, *10*, 10159-10169.
7. Kao, H.-M.; Liao, Y.-C., Direct Solid-State Nmr Observation of Tetrahedral Aluminum Fluorides in Zeolite HY Fluorinated by Ammonium Fluoride. *The Journal of Physical Chemistry C* **2007**, *111*, 4495-4498.
8. Qin, Z.; Melinte, G.; Gilson, J. P.; Jaber, M.; Bozhilov, K.; Boullay, P.; Mintova, S.; Ersen, O.; Valtchev, V., The Mosaic Structure of Zeolite Crystals. *Angewandte Chemie* **2016**, *128*, 15273-15276.
9. Xiao, D.; Xu, S.; Brownbill, N. J.; Paul, S.; Chen, L.-H.; Pawsey, S.; Aussenac, F.; Su, B.-L.; Han, X.; Bao, X., Fast Detection and Structural Identification of Carbocations on Zeolites by Dynamic Nuclear Polarization Enhanced Solid-State NMR. *Chemical Science* **2018**, *9*, 8184-8193.
10. Chowdhury, A. D.; Houben, K.; Whiting, G. T.; Mokhtar, M.; Asiri, A. M.; Al-Thabaiti, S. A.; Basahel, S. N.; Baldus, M.; Weckhuysen, B. M., Initial Carbon–Carbon Bond Formation During the Early Stages of the Methanol-to-Olefin Process Proven by Zeolite-Trapped Acetate and Methyl Acetate. *Angewandte Chemie* **2016**, *128*, 16072-16077.
11. Jiang, Y.; Huang, J.; Dai, W.; Hunger, M., Solid-State Nuclear Magnetic Resonance Investigations of the Nature, Property, and Activity of Acid Sites on Solid Catalysts. *Solid state nuclear magnetic resonance* **2011**, *39*, 116-141.